Cell Reports

Type 1 innate lymphoid cells regulate the onset of *Toxoplasma gondii*-induced neuroinflammation

Graphical abstract

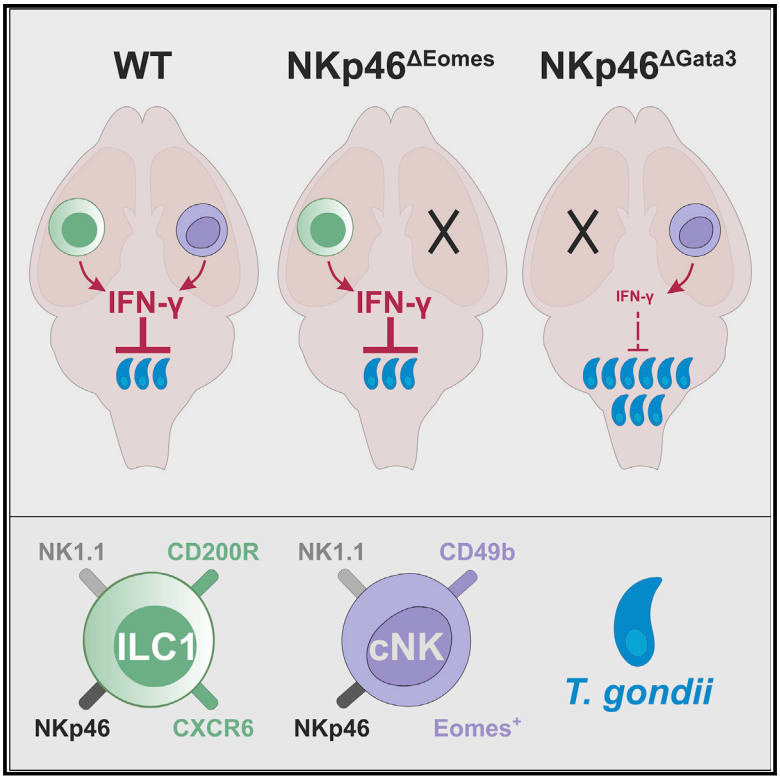

Highlights

- ILCs are present in distinct CNS compartments
- cNK cells and ILC1s accumulate during the onset of cerebral toxoplasmosis
- ILC1 loss results in reduced IFN-γ levels and increased parasite burden in the brain

Authors

Johannes Steffen, Stefanie Ehrentraut, Ute Bank, ..., Christoph S.N. Klose, Thomas Schüler, Ildiko Rita Dunay

Correspondence

ildikodunay@gmail.com

In brief

Steffen et al. report that ILC1s are an early source of IFN-γ in the CNS during the onset of cerebral *T. gondii* infection. Loss of ILC1s delays the production of IFN-γ-associated host defense factors and subsequent pathogen control.

Steffen et al., 2022, Cell Reports *38*, 110564
March 29, 2022
https://doi.org/10.1016/j.celrep.2022.110564

CellPress

Cell Reports

CellPress
OPEN ACCESS

Report

Type 1 innate lymphoid cells regulate the onset of *Toxoplasma gondii*-induced neuroinflammation

Johannes Steffen,[1] Stefanie Ehrentraut,[1] Ute Bank,[2] Aindrila Biswas,[1] Caio Andreeta Figueiredo,[1] Oliver Hölsken,[3,4] Henning Peter Düsedau,[1] Vladyslava Dovhan,[2] Laura Knop,[2] Jacqueline Thode,[1] Silvina Romero-Suárez,[5] Carmen Infante Duarte,[5] Jason Gigley,[6] Chiara Romagnani,[7,8] Andreas Diefenbach,[3,4] Christoph S.N. Klose,[9] Thomas Schüler,[2,11] and Ildiko Rita Dunay[1,10,11,12,*]

[1]Institute of Inflammation and Neurodegeneration, Health Campus Immunology, Infectiology, and Inflammation (GC-I[3]), Otto von Guericke University, Leipziger Straße 44, 39120 Magdeburg, Germany
[2]Institute of Molecular and Clinical Immunology, Health Campus Immunology, Infectiology, and Inflammation (GC-I[3]), Otto-von-Guericke University, Magdeburg, Germany
[3]Mucosal and Developmental Immunology, German Rheuma Research Center Berlin (DRFZ), Berlin, Germany
[4]Laboratory of Innate Immunity, Department of Microbiology, Infectious Diseases, and Immunology, Charité – Universitätsmedizin Berlin, Campus Benjamin Franklin, Berlin, Germany
[5]Institute for Medical Immunology, Charité – Universitätsmedizin Berlin, Berlin, Germany
[6]Department of Molecular Biology, University of Wyoming, Laramie, WY 82071, USA
[7]Innate Immunity, German Rheumatism Research Center Berlin (DRFZ), Berlin, Germany
[8]Medical Department I, Charité - Universitätsmedizin, Berlin, Germany
[9]Neuro-immune Interactions, Institute of Microbiology, Infectious Diseases, and Immunology, Charité – Universitätsmedizin, Berlin, Germany
[10]Center for Behavioral Brain Sciences, Magdeburg, Germany
[11]These authors contributed equally
[12]Lead contact
*Correspondence: ildikodunay@gmail.com
https://doi.org/10.1016/j.celrep.2022.110564

SUMMARY

Cerebral infections are restrained by a complex interplay of tissue-resident and recruited peripheral immune cells. Whether innate lymphoid cells (ILCs) are involved in the orchestration of the neuroinflammatory dynamics is not fully understood. Here, we demonstrate that ILCs accumulate in the cerebral parenchyma, the choroid plexus, and the meninges in the onset of cerebral *Toxoplasma gondii* infection. Antibody-mediated depletion of conventional natural killer (cNK) cells and ILC1s in the early stage of infection results in diminished cytokine and chemokine expression and increased cerebral parasite burden. Using cNK- and ILC1-deficient murine models, we demonstrate that exclusively the lack of ILC1s affects cerebral immune responses. In summary, our results provide evidence that ILC1s are an early source of IFN-γ and TNF in response to cerebral *T. gondii* infection, thereby inducing host defense factors and initiating the development of a neuroinflammatory response.

INTRODUCTION

Innate lymphoid cells (ILCs) comprise a heterogeneous population of immune cells, which have lately been characterized in the peripheral organs of mice and humans (Vivier et al., 2018). ILCs are present throughout the body and are predominantly enriched at mucosal surfaces, where they swiftly respond to environmental changes (Spits et al., 2013). Similar to the different subsets of $CD4^+$ T helper cells, ILCs can be classified into ILC1s, ILC2s, and ILC3s based on their functional properties and transcription factor expression profiles. Conventional natural killer (cNK) cells represent their cytotoxic counterpart and share similarities with $CD8^+$ T cells (Vivier et al., 2018). While both cNK cells and ILC1s produce inflammatory cytokines such as interferon (IFN)-γ to promote type 1 immune responses against intracellular pathogens (Colonna, 2018; Daussy et al., 2014), each cell type can have non-redundant, tissue-specific functions (Colonna, 2018; Weizman et al., 2017). For example, the reconstitution of alymphoid $Rag2^{-/-}Il2r\gamma^{-/-}$ mice with $NKp46^+NK1.1^+T\text{-}bet^+ROR\gamma t^-Eomes^-$ ILC1s restores IFN-γ/tumor necrosis factor (TNF)-related protection against *Toxoplasma gondii* infection in the ileum (Klose et al., 2014). The ILC1-dependent responses were associated with the enhanced recruitment of inflammatory $Ly6C^{hi}$ monocytes, suggesting that ILC1s, rather than cNK cells, are crucial for controlling intestinal *T. gondii* infection (Klose et al., 2014).

Accumulating evidence suggests that ILCs contribute to the initiation, regulation, and resolution of immune responses in various organs (Colonna, 2018; Vivier et al., 2018). However, due to the low ILC abundance in the central nervous system (CNS)

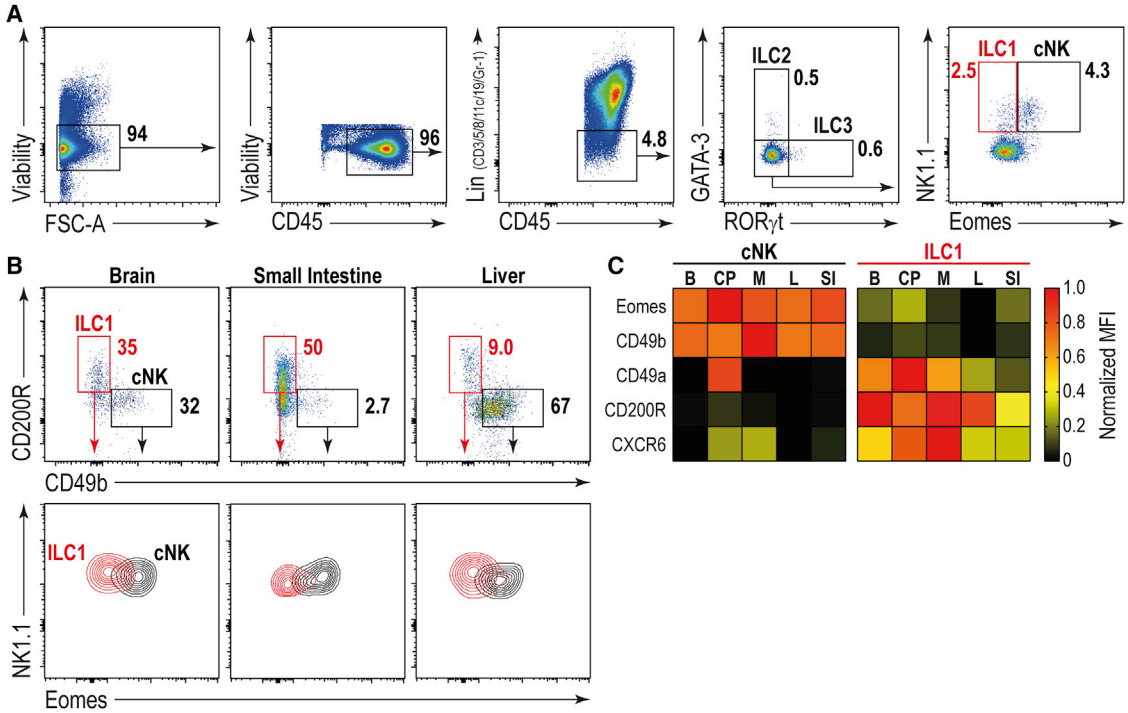

Figure 1. Characterization of innate lymphoid cell populations in the central nervous system compartments

(A and B) B6/WT mice were *T. gondii*- or (C) mock-infected; leukocytes were analyzed by flow cytometry. (B) Viable CD45$^+$lineage$^-$NK1.1$^+$NKp46$^+$ cells were analyzed for the expression of the indicated molecules to discriminate between CD200R$^+$CD49b$^-$Eomes^{lo} ILC1s and CD200R$^-$CD49b$^+$Eomes^{hi} cNKs.

(C) Heatmap shows normalized median fluorescence intensity (MFI) of indicated markers for cNK cells (CD49b$^+$) and ILC1s (CD200R$^+$) isolated from the brain parenchyma (B), choroid plexus (CP), meninges (M), liver (L), and small intestine (SI). The plots show (A) a representative sample or (B) concatenated samples (n = 10 mice).

(Kwong et al., 2017; Mrdjen et al., 2018; Romero-Suarez et al., 2019; Zelco et al., 2020), little is known regarding their role in tissue homeostasis, disease, and inflammation. Accordingly, we scrutinized the cerebral toxoplasmosis model (Figueiredo et al., 2022; French et al., 2021; Matta et al., 2021) to characterize the function of ILCs during pathogen-induced neuroinflammation.

Here, we show that NK1.1$^+$NKp46$^+$CD200R$^+$ ILC1s rather than NK1.1$^+$NKp46$^+$CD49b$^+$ cNK cells contribute to the early control of cerebral *T. gondii* infection. ILC1s accumulated in the CNS at the onset of the infection. Their antibody-mediated depletion was associated with reduced expression of IFN-γ-related host defense factors and delayed pathogen control. Correspondingly, ILC1-deficient mice displayed increased *T. gondii* burden in the brain due to the hampered IFN-γ expression. In contrast, the parasite-related immune responses remained unaltered in cNK-deficient mice. In summary, we demonstrate that ILC1s serve as an immediate source of antiparasitic cytokines at the very early stage of cerebral toxoplasmosis, thereby facilitating the subsequent adaptive immunity required for long-term pathogen control.

RESULTS

ILC1 accumulate in the brain during *T. gondii* infection-induced neuroinflammation

ILCs play a pivotal role in the initiation, regulation, and resolution of inflammation in multiple organs (Colonna, 2018; Spits et al., 2013; Vivier et al., 2018). However, not much is known about their function in the CNS, particularly in the course of infection-associated neuroinflammation. To address this issue, we infected mice with *T. gondii* and analyzed the dynamics of CD45$^+$lineage$^-$ innate immune cells by flow cytometry. To discriminate between different ILC subsets, we quantified differentially expressed cell surface markers and transcription factors (Klose and Diefenbach, 2014; McFarland et al., 2021; Vivier et al., 2018). Cerebral CD45$^+$lineage$^-$ cells were defined as ILC2s (GATA-3^{hi}), ILC3s (RORγt$^+$), ILC1s (NK1.1$^+$Eomes$^-$), and cNKs (NK1.1$^+$Eomes$^+$), respectively (Figure 1A). The discrimination between ILC1s and cNKs is still challenging since their gene expression profiles overlap and vary in a tissue-specific manner. Due to the lack of a unique cell surface marker (McFarland et al., 2021), a combination of CD49b (cNKs), CD49a, CD200R, and CXCR6 (ILC1s) was used to discriminate between cNKs and ILC1s (Figures 1B and 1C) (McFarland et al., 2021; Romero-Suarez et al., 2019; Weizman et al., 2017). Similar to their well-described counterparts in the periphery (liver and intestine), meningeal and brain parenchyma-derived NK1.1$^+$NKp46$^+$CD49b$^+$ cNKs expressed high levels of Eomes, but were negative for CD49a, CD200R, and CXCR6. On the contrary, cerebral and peripheral ILC1s were NK1.1$^+$NKp46$^+$CD200R$^+$CD49a$^+$CXCR6$^+$ but lacked Eomes and CD49b expression (Figure 1C).

In accordance with previous results (Kvestak et al., 2021; Kwong et al., 2017; Mrdjen et al., 2018; Romero-Suarez

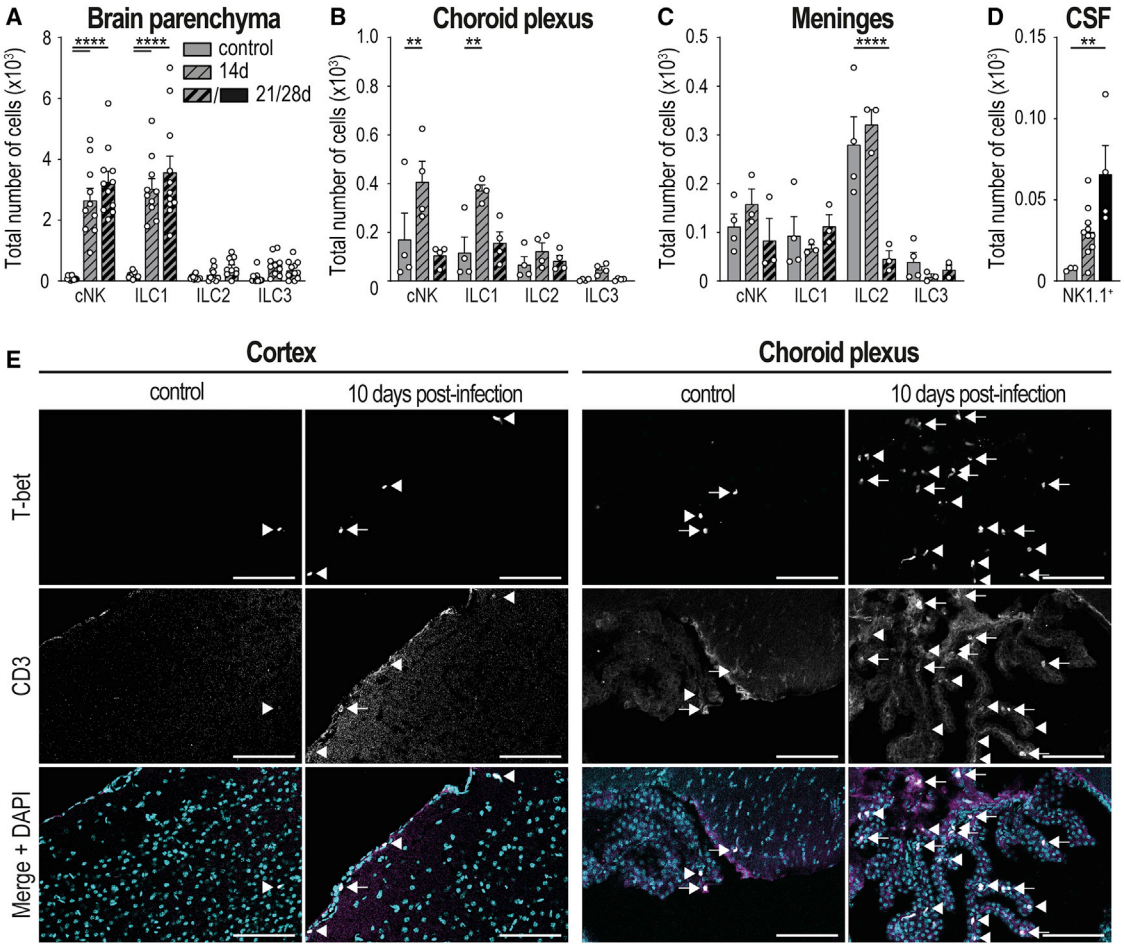

Figure 2. Dynamics of innate lymphoid cells in the CNS upon cerebral toxoplasmosis

(A–C) The absolute number of respective ILC subsets (as defined in Figure 1A) during steady state, 14, and 21 days post-infection in (A) brain parenchyma, (B) choroid plexus, and (C) meninges of *T. gondii*- or mock-infected (control) B6/WT mice.

(D) Viable $CD45^+NK1.1^+$ cells were analyzed in the CSF.

(E) Anatomical localization of cNKs/ILC1s ($T\text{-}bet^+CD3^-$) was analyzed in T-bet reporter mice (Tbx21-ZsGreen).

The bar graphs summarize results obtained in (A–C) 4 independent experiments (n = 10–13 mice), or (D) 3 independent experiments (n = 4–10 mice). Samples from choroid plexus, meninges, and CSF were pooled for staining where necessary (n = 2–5 mice per sample). The absolute cell numbers are presented as mean + SEM. The differences between groups were analyzed by (A–C) 2-way ANOVA followed by Dunnett's multiple comparisons test or (D) 1-way ANOVA followed by Tukey's multiple comparisons test (**$p \leq 0.01$; ****$p \leq 0.0001$). (E) Scale bars = 100 μm.

et al., 2019; Van Hove et al., 2019; Zelco et al., 2020), small populations of ILCs were present in different CNS compartments in the steady state (brain parenchyma, choroid plexus, and meninges; Figures 2A–2C and 2E). In the brain parenchyma, the number of cNKs and ILC1s persistently increased during the acute and chronic phases of cerebral toxoplasmosis (14–21 days post-infection; Figure 2A). In the choroid plexus, an established entry point for leukocytes to the inflamed CNS parenchyma (Schwartz and Baruch, 2014; Xiao et al., 2018), the number of cNKs and ILC1s significantly increased during the acute infection phase and subsequently decreased to basal levels (Figure 2B). Consistent with previous reports (Fung et al., 2020; Gadani et al., 2017), cerebral ILC2s represented the most abundant ILC population in the meninges under steady-state conditions but decreased in the course of infection (Figure 2C).

In addition, the cerebrospinal fluid (CSF) contained an increased amount of $CD45^+NK1.1^+$ cells upon *T. gondii* infection (Figure 2D). To visualize the anatomical location of cerebral cNKs and ILC1s, we used Tbx21-ZsGreen mice (Zhu et al., 2012), expressing the green fluorescent protein ZsGreen (ZsG) under the control of the *Tbx21* promoter, thus labeling both $CD3^+$ T lymphocytes and $CD3^-$ cNKs/ILC1s. ZsG^+CD3^- cNKs/ILC1s were present in the brain parenchyma under steady-state conditions and expanded during cerebral *T. gondii* infection (Figure 2E). In the choroid plexus, both ZsG^+CD3^+ and ZsG^+CD3^- cells accumulated during infection, suggesting their distinct recruitment to this site.

In summary, we show that $NK1.1^+NKp46^+Eomes^+CD49b^+$ cNK cells and $NK1.1^+NKp46^+CD49a^+CD200R^+CXCR6^+$ ILC1s present in the CNS phenotypically resemble their peripheral

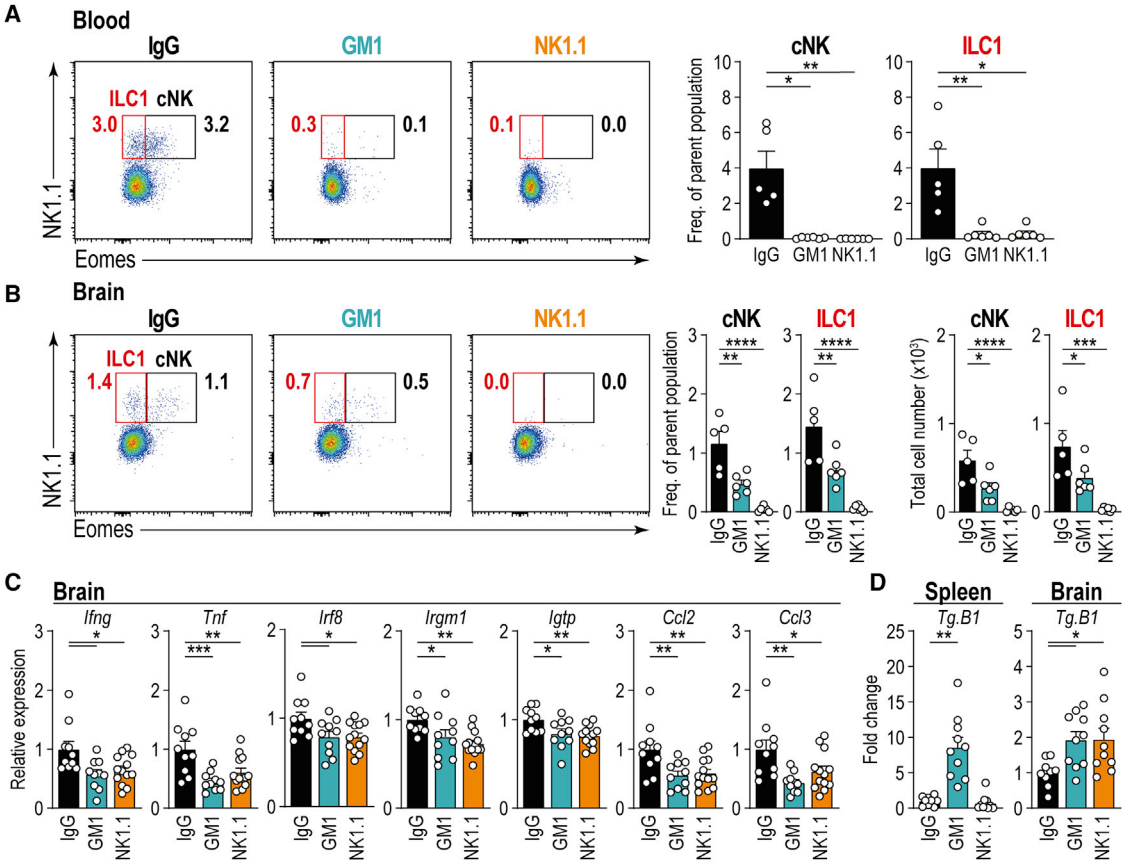

Figure 3. The depletion of group 1 ILCs exacerbates cerebral toxoplasmosis

B6/WT mice were *T. gondii*-infected, NK1.1^{+}Eomes^{+} and NK1.1^{+}Eomes^{-} cells were depleted by *intraperitoneal* (*i.p.*) application of either 50 μg anti-asialo GM1 (GM1), 200 μg anti-NK1.1 (NK1.1), or an equal amount of respective immunoglobulin G (IgG) isotype at 7, 10, and 13 days post-infection.

(A and B) Representative flow cytometric analyses of (A) blood (gated on live CD45^{+}CD4^{-}CD8^{-}lineage^{-}GATA-3^{lo}RORγt^{-}) and (B) brain (gated on live CD45^{+}lineage^{-}GATA-3^{lo}RORγt^{-}) are shown for IgG-, GM1-, and NK1.1-treated animals.

(C and D) Relative mRNA levels of indicated genes and fold change in parasite load in the brain and periphery were analyzed at (C) 10 and (D) 14 days post-infection.

The plots (A and B) show concatenated samples (n = 5–6 mice). The bar graphs show (A and B) representative results obtained in 2 independent experiments, or (C and D) summarize results from both experiments (n = 9–13 mice). The IgG group shows pooled data of both isotypes. Data are presented as mean + SEM. The differences between groups were analyzed by (A–C: *Tnf*, *Irf8*, *Irgm1*, *Igtp*, *Ccl2*, and *Ccl3*, and D: Brain) 1-way ANOVA followed by Dunnett's multiple comparisons test or (C: *Ifng*; D: spleen) the Kruskal-Wallis test followed by Dunn's multiple comparisons test (*p ≤ 0.05; **p ≤ 0.01; ***p ≤ 0.001; ****p ≤ 0.0001).

See also Figure S1.

counterparts. Furthermore, *T. gondii* infection alters the abundance of cerebral ILCs, particularly cNKs and ILC1s.

Depletion of NK1.1^{+} cells exacerbates cerebral toxoplasmosis

Previous studies have shown that parasite control critically relies on IFN-γ (Suzuki et al., 1988), the expression of host defense factors (Taylor et al., 2000), the recruitment of inflammatory Ly6C^{hi} monocytes (Biswas et al., 2015; Dunay et al., 2008), and the induction of T helper 1 (Th1)-associated adaptive immunity (Oldenhove et al., 2009). Since peripheral cNKs and ILC1s produce IFN-γ in response to *T. gondii* (Klose et al., 2014; Park et al., 2019) and both cell types accumulate in the infected brain (Figure 2), we hypothesized that they contribute to early pathogen control in the CNS. To address this issue, we depleted cNK cells and ILC1s using anti-asialo GM1 or anti-NK1.1 antibodies (Ivanova et al., 2020; Kvestak et al., 2021; Nabekura et al., 2020). *T. gondii*-infected mice were treated with depleting or isotype-matched control antibodies every third day, starting 7 days post-infection. Administration of either anti-asialo GM1 or anti-NK1.1 substantially reduced NK1.1^{+}Eomes^{+} cNK cells and NK1.1^{+}Eomes^{-} ILC1s in the blood and the brain (Figures 3A and 3B), accompanied by the decreased expression of *Ifng* and *Tnf* (Figure 3C). To confirm impaired IFN-γ signaling, the expression of IFN-γ-regulated, cell-intrinsic host defense factors *Irf8*, *Irgm1*, and *Igtp* was analyzed (Figure 3C). The absence of cNKs/ILC1s resulted in reduced expression of interferon regulatory factor 8 (*Irf8*), essential for innate resistance against intracellular pathogens (Lopez-Yglesias et al., 2021), as well as *Irgm1* and *Igtp*, which mediate early, cell-autonomous resistance to

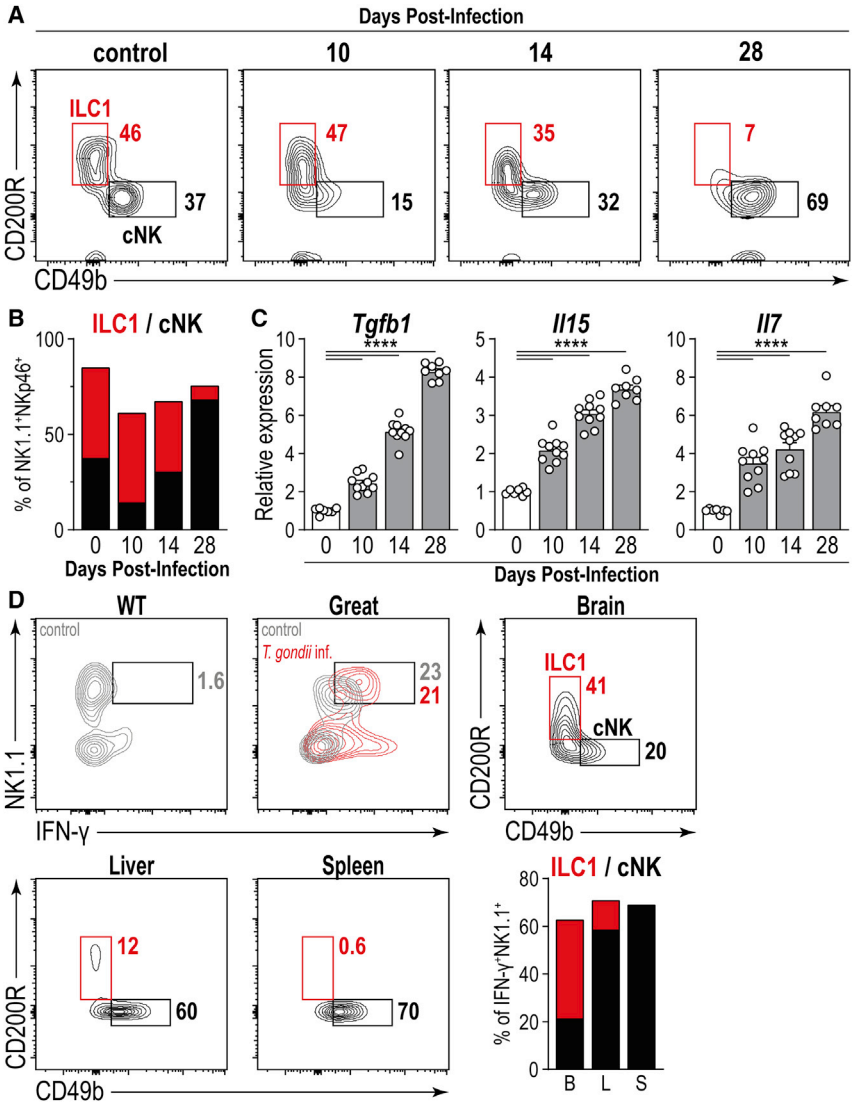

Figure 4. Expansion of cerebral ILC1s upon *T. gondii* infection

(A and B) Frequencies of cNK cells (CD49b$^+$) and ILC1s (CD200R$^+$) in the brain were determined at indicated time points post-infection after gating on live CD45$^+$lineage$^-$NK1.1$^+$NKp46$^+$.

(C) Relative mRNA levels of TGF-β, IL-15, and IL-7 in the brain.

(D) Cells isolated from the brain (B), liver (L), and spleen (S) of *T. gondii*-infected IFN-γ eYFP reporter (Great) mice 10 days post-infection were gated on live CD45$^+$lineage$^-$NKp46$^+$eYFP$^+$NK1.1$^+$ to identify cNK cells (CD49b$^+$) and ILC1s (CD200R$^+$).

The plots (A and D) show concatenated samples (n = 2–10 mice). The bar graphs summarize results obtained in (B) and (C) 6 independent experiments (n = 7–10 mice), or (D) 1 experiment (n = 2–6 mice). The data are presented as mean + SEM. The differences between groups were analyzed by (C) 1-way ANOVA followed by Dunnett's multiple comparisons test (****$p \leq 0.0001$). (A and B) The data from the brain are also shown in Figure 1 for organ comparison.

See also Figures S2 and S3.

T. gondii infection (Boehm et al., 1998; Taylor et al., 2000). ILC1s were previously shown to promote the recruitment of Ly6C^{hi} inflammatory monocytes during intestinal *T. gondii* infection (Klose et al., 2014), a process depending on C-C motif chemokine ligand 2 (CCL2) (Dunay et al., 2008; Robben et al., 2005) and CCL3 (Schulthess et al., 2012). Depletion of cNKs/ILC1s was associated with a significant reduction in *Ccl2* and *Ccl3* expression (Figure 3C), reduced numbers of inflammatory Ly6C^{hi} monocytes (Figures S1C and S1D), and an increased parasite burden in the brain (Figure 3D). In the spleen, only anti-asialo GM1 but not anti-NK1.1 treatment significantly impaired pathogen clearance (Figure 3D), which at this time point vitally depends on CD4$^+$ and CD8$^+$ T cells in the periphery (Matta et al., 2021). Since anti-asialo GM1 treatment may also affect T cells (Ivanova et al., 2019, 2020), we analyzed peripheral blood lymphocytes and detected that the administration of anti-asialo GM1, but not anti-NK1.1, decreased the frequencies of CD4$^+$ and CD8$^+$ cells (Figures S1A and S1B).

The data presented so far demonstrate that NK1.1$^+$ innate immune cells accumulate in the *T. gondii*-infected brain, contribute to IFN-γ-related immunity, and control pathogen load. To define the relative importance of cerebral cNKs and ILC1s, we determined the temporal dynamics in NK1.1$^+$NKp46$^+$ cells during toxoplasmosis. While distinct populations of CD49b$^+$ cNKs and CD200R$^+$ ILC1s were present in the brain at steady state, cerebral toxoplasmosis induced increased heterogeneity within the NK1.1$^+$NKp46$^+$ compartment (Figures 4A and S2). This is particularly evident within the CD49b$^+$ fraction, where CD49b$^+$CD49a$^+$Eomes$^+$ and CD49b$^+$CD49a$^+$Eomes$^-$ cells increased during the course of infection (Figure S2). However, in steady state and in the early to acute infection phase (10–14 days post-infection), CD200R$^+$ ILC1s constitute the main fraction of the cerebral NK1.1$^+$NKp46$^+$ cells (Figures 4A and 4B). Their *T. gondii*-associated accumulation may be facilitated by transforming growth factor (TGF)-β, interleukin (IL)-15, and IL-7 (Figure 4C), tissue-derived factors promoting the maintenance, survival, and plasticity of cNK cells and ILC1s (Cortez et al., 2016; Gao et al., 2017; Park et al., 2019; Sheikh and Abraham, 2019), which were continuously upregulated in the course of the infection (Figure 4C).

Next, we analyzed the functional state of cerebral ILC1s and cNKs using IFN-γ-reporter mice (Great) (Reinhardt et al., 2009) expressing enhanced yellow fluorescent protein (eYFP) under the control of the *Ifng* promoter. Ten days post-infection, leukocytes were isolated from the brains, spleens, and livers of *T. gondii*-infected reporter mice. Without further re-stimulation, EYFP expression was compared to non-infected wild-type

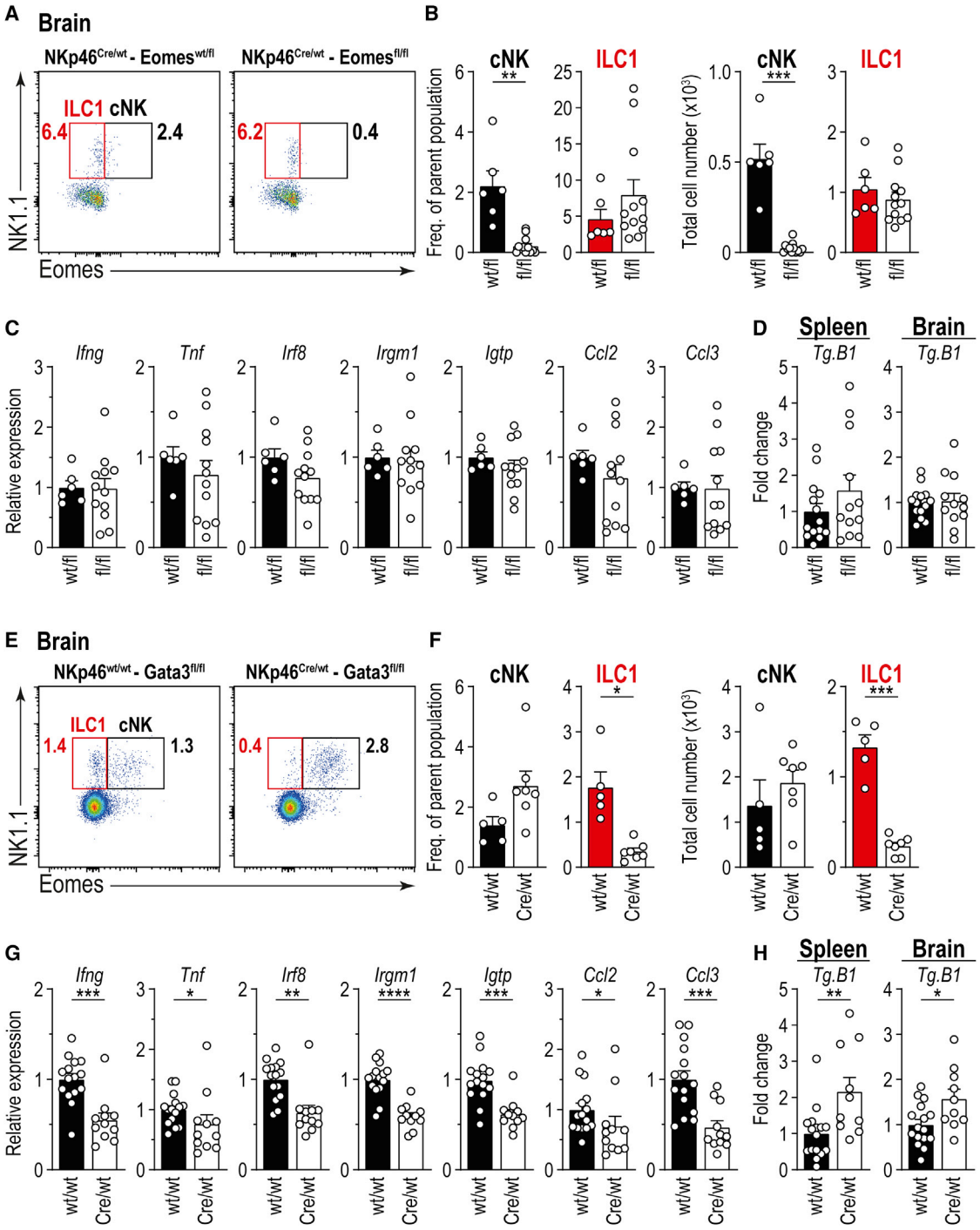

Figure 5. Cerebral ILC1s restrict cerebral *T. gondii* infection

(A–D) *NKp46*$^{Cre/wt}$*Eomes*$^{wt/fl}$ (wt/fl) and *NKp46*$^{Cre/wt}$*Eomes*$^{fl/fl}$ (fl/fl) or (E–H) *NKp46*$^{wt/wt}$*Gata3*$^{fl/fl}$ (wt/wt) and *NKp46*$^{Cre/wt}$*Gata3*$^{fl/fl}$ (Cre/wt) mice were *T. gondii* infected, and analyzed at (A–C and E–G) 10 or (D and H) 14 days post-infection.

(A and E) Flow cytometric analysis of live CD45^{+}lineage^{-}GATA-3^{lo}RORγt^{-} cells.

(B and F) Frequency and total cell number of cNKs (NK1.1^{+}Eomes^{+}) cells and ILC1s (NK1.1^{+}Eomes^{-}) in the brain.

(C, D, G, and H) Relative mRNA levels of indicated genes in the brain (C and G) and (D and H) fold change in *T. gondii* load in brain and spleen.

The data represent (A–C) 2 or (D–H) 3 independent experiments (n = 6–16 mice). The plots (A and E) show concatenated samples (n = 4–7 mice). The bar graphs show (B and F) representative or (C, D, G, and H) summarized results obtained in (A–C) 2 independent experiments (n = 6–16 mice) or (E, G, and H) 3 independent

(legend continued on next page)

(WT) and reporter mice (Figure 4D). In the brains of infected reporter mice, the majority of NK1.1^{+}NKp46^{+} cells producing high levels of eYFP were CD200R^{+} ILC1s. Their ability to produce IFN-γ and TNF was confirmed in a separate experiment (Figure S3). Contrary to the CNS, CD49b^{+} cNK cells were the main producers of IFN-γ in the liver and spleen (Figure 4D). Hence, our data suggest a specific function of IFN-γ-producing ILC1s in the early phase of cerebral *T. gondii* infection.

Cerebral ILC1s modulate *T. gondii*-induced neuroinflammation

After the detection of IFN-γ-producing cerebral cNK cells and ILC1s (Figures 4D and S3), we next examined their relative contribution to pathogen control. Therefore, we infected cNK-deficient *NKp46*$^{Cre/wt}$*Eomes*$^{fl/fl}$ mice (Bank et al., 2020) and corresponding littermate controls with *T. gondii* and determined the frequencies of cNK cells and ILC1s in infected brains. In accordance with previous reports (Kwong et al., 2017; Weizman et al., 2017), cNK cell numbers were strongly decreased in *NKp46*$^{Cre/wt}$*Eomes*$^{fl/fl}$ mice, while the abundance of cerebral ILC1s remained unaffected (Figures 5A and 5B). In the initial infection phase, parasite burden remained unaltered in the brains of infected cNK-deficient animals as compared to littermate controls (Figures 5D and S4D). The expression of *Ifng* and *Tnf* as well as *Irf8*, *Irgm1*, *Igtp*, *Ccl2*, and *Ccl3* were indistinguishable between both experimental groups (Figure 5C). Together, these data suggest that cNK cells are of minor importance for initiating the inflammatory response and early parasite control in the CNS.

To study the role of cerebral ILC1s, we used cNK-competent, ILC1-deficient *NKp46*$^{Cre/wt}$*Gata3*$^{fl/fl}$ mice (Ali et al., 2016; Klose et al., 2014; Figures 5E, 5F, S5A, and S5B). At day 10 post-infection with *T. gondii*, *Ifng* and *Tnf* expression was reduced in *NKp46*$^{Cre/wt}$*Gata3*$^{fl/fl}$ mice as compared to ILC1-competent controls (Figure 5G). Correspondingly, the expression of IFN-γ-regulated genes, such as *Irf8*, *Irgm1*, and *Igtp*, as well as the chemokines *Ccl2* and *Ccl3,* was significantly decreased in ILC1-deficient mice. Furthermore, parasite burden in the brain and the periphery of *NKp46*$^{Cre/wt}$*Gata3*$^{fl/fl}$ mice exceeded those of ILC1-competent littermates (Figure 5H). To exclude functional defects of *NKp46*$^{Cre/wt}$*Gata3*$^{fl/fl}$ cNKs, we analyzed their IFN-γ production in comparison to WT controls. As shown in Figures S5C and S5D, IFN-γ production was indistinguishable between both groups. Thus, ILC1s, but not cNKs, appear to be crucial for the very early production of IFN-γ, induction of host defense factors, and subsequent pathogen control in response to cerebral *T. gondii* infection.

DISCUSSION

After infection with *T. gondii,* host survival depends on a complex and organ-specific interplay between innate and adaptive immune cells. The function of different immune cell subsets, including ILCs, has been extensively studied in the periphery (Dunay et al., 2008; Dunay and Sibley, 2010; Klose et al., 2014; Kugler et al., 2016; Park et al., 2019; Snyder and Denkers, 2020; Yarovinsky, 2014). However, the relative contribution of ILCs to the early control of cerebral *T. gondii* infection has remained elusive.

Upon challenge with *T. gondii*, vaccinated WT mice succumb after anti-asialo GM1-mediated depletion of cNK and T cells (Ivanova et al., 2019). On the contrary, the data presented here demonstrate that anti-asialo GM1 treatment in the early phase of a primary *T. gondii* infection does not affect host survival. Hence, cNK and T cells appear to be crucial at later time points, but not at the onset of the cerebral infection.

A rapid IFN-γ response is essential to mediate the activation of resident immune cells and prevent the proliferation of fast-replicating tachyzoites (Suzuki, 2020). ILC1s represent important IFN-γ producers that act as a first line of defense against infections with viruses, bacteria, and parasites (Vivier et al., 2018). The timely induction of an IFN-γ response is of great importance in *T. gondii* infection, and delayed production increases parasite burden, mitigates monocyte activation, and decreases host survival (Hou et al., 2011; Suzuki, 2020). Here, we provide evidence that the protective effects of IFN-γ-producing ILC1s are not limited to the intestinal mucosa but are also evident in the CNS. Using two independent experimental systems, we demonstrate that the lack of ILC1s is associated with the reduced expression of (1) IFN-γ, (2) IFN-γ-dependent host defense factors, (3) impaired recruitment of protective Ly6C^{hi} monocytes, and consequently, (4) increased pathogen burden. Thus, our data suggest that ILC1s rather than cNKs are important for the early control of cerebral toxoplasmosis. This interpretation is further supported by the early accumulation of ILC1s in *T. gondii*-infected brains.

In our experiments, the systemic depletion of IFN-γ-producing NK1.1^{+} cells impaired host defense and increased parasite burden in the brain. Since different cellular sources of IFN-γ are known to exert complex and non-redundant roles in host defense, we used cNK- and ILC1-deficient animals to decipher their relative contributions (Klose et al., 2014; Kwong et al., 2017; Weizman et al., 2017). In cNK-deficient *NKp46*$^{Cre/wt}$*Eomes*$^{fl/fl}$ mice, the IFN-γ response was not significantly altered, indicating that IFN-γ from mature cNK cells is of limited importance for the initial control of cerebral toxoplasmosis. On the contrary, the induction of IFN-γ, host defense factors, recruitment of Ly6C^{hi} monocytes, and pathogen control were impaired in infected ILC1-deficient *NKp46*$^{Cre/wt}$*Gata3*$^{fl/fl}$ mice. In summary, our findings reveal that ILC1s play an important role in orchestrating the development of the early cytokine-mediated immune responses in the CNS. Cerebral ILC1s serve as an early line of defense, limiting the dissemination of the intracellular parasite *T. gondii*.

Limitations of the study

The elimination of ILC1 subsets has inherent limitations. Antibody-mediated depletion (e.g., anti-asialo GM1 treatment) can

experiments (n = 10–16 mice). The data are presented as mean + SEM. The differences between groups were analyzed by (B: total cell number, G: *Irgm1*, *Ccl3*; H: brain) unpaired t test, (B: Freq.; F: Freq., total cell number) t test with Welch's correction, or (G: *Ifng*, *Tnf*, *Irf8*, *Igtp*, and *Ccl2*; H: spleen) Mann-Whitney test with (*p ≤ 0.05; **p ≤ 0.01; ***p ≤ 0.001; ****p ≤ 0.0001).
See also Figures S4 and S5.

exert off-target effects and may alter immune responses via the modulation of frequencies and/or function of non-ILCs (Ivanova et al., 2019). Accordingly, we used cNK- and ILC1-deficient mice to determine the relative importance of the different ILC subsets. Genetic ablation of particular cells is not necessarily complete or may entail compensatory mechanisms by other immune cells, which cannot formally be excluded for cNK-deficient *NKp46*$^{Cre/wt}$*Eomes*$^{fl/fl}$ mice. Therefore, we used ILC1-deficient *NKp46*$^{Cre/wt}$*Gata3*$^{fl/fl}$ mice to complement the aforementioned approaches with a third, independent experimental system. However, GATA-3 inactivation in NKp46^{+} cells not only causes the loss of ILC1s but was also shown to impair IFN-γ production by cNKs in some experimental systems (Ali et al., 2016; Samson et al., 2003). Although we did not detect significant changes in IFN-γ production upon *ex vivo* re-stimulation of cNKs (Figures S5C and S5D), we cannot entirely exclude that, for example, altered IFN-γ responses by non-ILC1s affected the results obtained with infected *NKp46*$^{Cre/wt}$*Gata3*$^{fl/fl}$ mice. Despite the individual limitations of each experimental system, their complementary use supports our conclusion of an important function of ILC1s for the early control of cerebral toxoplasmosis, whereas cNKs are of minor importance.

STAR★METHODS

Detailed methods are provided in the online version of this paper and include the following:

- KEY RESOURCES TABLE
- RESOURCE AVAILABILITY
  - Lead contact
  - Materials availability
  - Data and code availability
- EXPERIMENTAL MODEL AND SUBJECT DETAILS
  - Mice
- METHOD DETAILS
  - Cell depletion
  - Organ collection
  - Cell isolation
  - Flow cytometric analysis
  - RNA, DNA isolation and RT-qPCR
  - Immunofluorescence
- QUANTIFICATION AND STATISTICAL ANALYSIS

SUPPLEMENTAL INFORMATION

Supplemental information can be found online at https://doi.org/10.1016/j.celrep.2022.110564.

ACKNOWLEDGMENTS

We thank Petra Grüneberg, Dr. Sarah Abidat Schneider, Jana Giese, and Karin Oberle for their exceptional technical assistance, and Mathias Wolff and Daniela Otte for excellent animal care. This work was supported by grants from the German Research Foundation to C.R. (DFG SPP1937), A.D. (DFG SPP1937), C.S.N.K. (DFG KL 2963/2-1 and KL 2963/3-1), T.S. (DFG SPP1937 and SCHU 2326/2-2), and I.R.D. (DFG SPP1937, DU1112/5-1, and RTG 2413 SynAGE), and the European Research Council Starting Grant to C.S.N.K. (ERCEA; 803087).

AUTHOR CONTRIBUTIONS

Conceptualization, I.R.D.; methodology, I.R.D., T.S., C.S.N.K., and A.D.; validation, J.S., A.B., S.E., C.A.F., I.R.D., and T.S.; formal analysis, J.S., A.B., S.E., and C.A.F.; investigation, J.S., S.E., U.B., A.B., C.A.F., H.P.D., V.D., L.K., and J.T.; resources, A.D., O.H., C.S.N.K., S.R.-S., and C.I.D.; writing – original draft, J.S., I.R.D., and T.S.; writing – review & editing, A.D., C.S.N.K., C.R., J.G., S.E., C.A.F., H.P.D., V.D., L.K., and O.H.; visualization, J.S., T.S., and I.R.D.; supervision, I.R.D. and T.S.; funding acquisition, I.R.D., T.S., A.D., C.S.N.K., and C.R.

DECLARATION OF INTERESTS

The authors declare no competing interests.

INCLUSION AND DIVERSITY

One or more of the authors of this paper self-identifies as a member of the LGBTQ+ community.

Received: March 12, 2021
Revised: December 21, 2021
Accepted: March 3, 2022
Published: March 29, 2022

REFERENCES

Ali, A.K., Oh, J.S., Vivier, E., Busslinger, M., and Lee, S.H. (2016). NK cell-specific Gata3 ablation identifies the maturation program required for bone marrow exit and control of proliferation. J. Immunol. *196*, 1753–1767. https://doi.org/10.4049/jimmunol.1501593.

Amsen, D., Antov, A., Jankovic, D., Sher, A., Radtke, F., Souabni, A., Busslinger, M., McCright, B., Gridley, T., and Flavell, R.A. (2007). Direct regulation of Gata3 expression determines the T helper differentiation potential of Notch. Immunity *27*, 89–99. https://doi.org/10.1016/j.immuni.2007.05.021.

Bank, U., Deiser, K., Plaza-Sirvent, C., Osbelt, L., Witte, A., Knop, L., Labrenz, R., Jansch, R., Richter, F., Biswas, A., et al. (2020). c-FLIP is crucial for IL-7/IL-15-dependent NKp46(+) ILC development and protection from intestinal inflammation in mice. Nat. Commun. *11*, 1056. https://doi.org/10.1038/s41467-020-14782-3.

Biswas, A., Bruder, D., Wolf, S.A., Jeron, A., Mack, M., Heimesaat, M.M., and Dunay, I.R. (2015). Ly6C(high) monocytes control cerebral toxoplasmosis. J. Immunol. *194*, 3223–3235. https://doi.org/10.4049/jimmunol.1402037.

Boehm, U., Guethlein, L., Klamp, T., Ozbek, K., Schaub, A., Futterer, A., Pfeffer, K., and Howard, J.C. (1998). Two families of GTPases dominate the complex cellular response to IFN-gamma. J. Immunol. *161*, 6715–6723.

Butcher, B.A., Fox, B.A., Rommereim, L.M., Kim, S.G., Maurer, K.J., Yarovinsky, F., Herbert, D.R., Bzik, D.J., and Denkers, E.Y. (2011). *Toxoplasma gondii* rhoptry kinase ROP16 activates STAT3 and STAT6 resulting in cytokine inhibition and arginase-1-dependent growth control. PLoS Pathog. *7*, e1002236. https://doi.org/10.1371/journal.ppat.1002236.

Colonna, M. (2018). Innate lymphoid cells: diversity, plasticity, and unique functions in immunity. Immunity *48*, 1104–1117. https://doi.org/10.1016/j.immuni.2018.05.013.

Cortez, V.S., Cervantes-Barragan, L., Robinette, M.L., Bando, J.K., Wang, Y., Geiger, T.L., Gilfillan, S., Fuchs, A., Vivier, E., Sun, J.C., et al. (2016). Transforming growth factor-beta signaling guides the differentiation of innate lymphoid cells in salivary glands. Immunity *44*, 1127–1139. https://doi.org/10.1016/j.immuni.2016.03.007.

Daussy, C., Faure, F., Mayol, K., Viel, S., Gasteiger, G., Charrier, E., Bienvenu, J., Henry, T., Debien, E., Hasan, U.A., et al. (2014). T-bet and Eomes instruct the development of two distinct natural killer cell lineages in the liver and in the bone marrow. J. Exp. Med. *211*, 563–577. https://doi.org/10.1084/jem.20131560.

Dunay, I.R., Damatta, R.A., Fux, B., Presti, R., Greco, S., Colonna, M., and Sibley, L.D. (2008). Gr1(+) inflammatory monocytes are required for mucosal resistance to the pathogen *Toxoplasma gondii*. Immunity *29*, 306–317. https://doi.org/10.1016/j.immuni.2008.05.019.

Dunay, I.R., and Sibley, L.D. (2010). Monocytes mediate mucosal immunity to *Toxoplasma gondii*. Curr. Opin. Immunol. *22*, 461–466. https://doi.org/10.1016/j.coi.2010.04.008.

Dusedau, H.P., Kleveman, J., Figueiredo, C.A., Biswas, A., Steffen, J., Kliche, S., Haak, S., Zagrebelsky, M., Korte, M., and Dunay, I.R. (2019). p75(NTR) regulates brain mononuclear cell function and neuronal structure in Toxoplasma infection-induced neuroinflammation. Glia *67*, 193–211. https://doi.org/10.1002/glia.23553.

Figueiredo, C.A., Steffen, J., Morton, L., Arumugam, S., Liesenfeld, O., Deli, M.A., Kroger, A., Schuler, T., and Dunay, I.R. (2022). Immune response and pathogen invasion at the choroid plexus in the onset of cerebral toxoplasmosis. J. Neuroinflammation *19*, 17. https://doi.org/10.1186/s12974-021-02370-1.

French, T., Israel, N., Dusedau, H.P., Tersteegen, A., Steffen, J., Cammann, C., Topfstedt, E., Dieterich, D., Schuler, T., Seifert, U., and Dunay, I.R. (2021). The immunoproteasome subunits LMP2, LMP7 and MECL-1 are crucial along the induction of cerebral toxoplasmosis. Front Immunol. *12*, 619465. https://doi.org/10.3389/fimmu.2021.619465.

Fung, I.T.H., Sankar, P., Zhang, Y., Robison, L.S., Zhao, X., D'Souza, S.S., Salinero, A.E., Wang, Y., Qian, J., Kuentzel, M.L., et al. (2020). Activation of group 2 innate lymphoid cells alleviates aging-associated cognitive decline. J. Exp. Med. *217*, e20190915. https://doi.org/10.1084/jem.20190915.

Gadani, S.P., Smirnov, I., Smith, A.T., Overall, C.C., and Kipnis, J. (2017). Characterization of meningeal type 2 innate lymphocytes and their response to CNS injury. J. Exp. Med. *214*, 285–296. https://doi.org/10.1084/jem.20161982.

Gao, Y., Souza-Fonseca-Guimaraes, F., Bald, T., Ng, S.S., Young, A., Ngiow, S.F., Rautela, J., Straube, J., Waddell, N., Blake, S.J., et al. (2017). Tumor immunoevasion by the conversion of effector NK cells into type 1 innate lymphoid cells. Nat. Immunol. *18*, 1004–1015. https://doi.org/10.1038/ni.3800.

Grote, D., Souabni, A., Busslinger, M., and Bouchard, M. (2006). Pax 2/8-regulated Gata 3 expression is necessary for morphogenesis and guidance of the nephric duct in the developing kidney. Development *133*, 53–61. https://doi.org/10.1242/dev.02184.

Hou, B., Benson, A., Kuzmich, L., DeFranco, A.L., and Yarovinsky, F. (2011). Critical coordination of innate immune defense against *Toxoplasma gondii* by dendritic cells responding via their Toll-like receptors. Proc. Natl. Acad. Sci. U S A *108*, 278–283. https://doi.org/10.1073/pnas.1011549108.

Ivanova, D.L., Denton, S.L., and Gigley, J. (2019). Anti-Asialo GM1 treatment during secondary *Toxoplasma gondii* infection is lethal and depletes T cells. J. Immunol. *202*, 190.53. https://doi.org/10.1101/550608.

Ivanova, D.L., Krempels, R., Denton, S.L., Fettel, K.D., Saltz, G.M., Rach, D., Fatima, R., Mundhenke, T., Materi, J., Dunay, I.R., and Gigley, J.P. (2020). NK cells negatively regulate CD8 T cells to promote immune exhaustion and chronic toxoplasma gondii infection. Front. Cell Infect. Microbiol. *10*, 313. https://doi.org/10.3389/fcimb.2020.00313.

Klose, C.S., and Diefenbach, A. (2014). Transcription factors controlling innate lymphoid cell fate decisions. Curr. Top Microbiol. Immunol. *381*, 215–255. https://doi.org/10.1007/82_2014_381.

Klose, C.S.N., Flach, M., Mohle, L., Rogell, L., Hoyler, T., Ebert, K., Fabiunke, C., Pfeifer, D., Sexl, V., Fonseca-Pereira, D., et al. (2014). Differentiation of type 1 ILCs from a common progenitor to all helper-like innate lymphoid cell lineages. Cell *157*, 340–356. https://doi.org/10.1016/j.cell.2014.03.030.

Kugler, D.G., Flomerfelt, F.A., Costa, D.L., Laky, K., Kamenyeva, O., Mittelstadt, P.R., Gress, R.E., Rosshart, S.P., Rehermann, B., Ashwell, J.D., et al. (2016). Systemic toxoplasma infection triggers a long-term defect in the generation and function of naive T lymphocytes. J. Exp. Med. *213*, 3041–3056. https://doi.org/10.1084/jem.20151636.

Kunis, G., Baruch, K., Rosenzweig, N., Kertser, A., Miller, O., Berkutzki, T., and Schwartz, M. (2013). IFN-gamma-dependent activation of the brain's choroid plexus for CNS immune surveillance and repair. Brain *136*, 3427–3440. https://doi.org/10.1093/brain/awt259.

Kvestak, D., Juranic Lisnic, V., Lisnic, B., Tomac, J., Golemac, M., Brizic, I., Indenbirken, D., Cokaric Brdovcak, M., Bernardini, G., Krstanovic, F., et al. (2021). J. Exp. Med. *218*, e20201503. https://doi.org/10.1084/jem.20201503.

Kwong, B., Rua, R., Gao, Y., Flickinger, J., Jr., Wang, Y., Kruhlak, M.J., Zhu, J., Vivier, E., McGavern, D.B., and Lazarevic, V. (2017). T-bet-dependent NKp46(+) innate lymphoid cells regulate the onset of TH17-induced neuroinflammation. Nat. Immunol. *18*, 1117–1127. https://doi.org/10.1038/ni.3816.

Lee, J.D., Levin, S.C., Willis, E.F., Li, R., Woodruff, T.M., and Noakes, P.G. (2018). Complement components are upregulated and correlate with disease progression in the TDP-43(Q331K) mouse model of amyotrophic lateral sclerosis. J. Neuroinflammation *15*, 171. https://doi.org/10.1186/s12974-018-1217-2.

Liesenfeld, O., Dunay, I.R., and Erb, K.J. (2004). Infection with *Toxoplasma gondii* reduces established and developing Th2 responses induced by Nippostrongylus brasiliensis infection. Infect. Immun. *72*, 3812–3822. https://doi.org/10.1128/IAI.72.7.3812-3822.2004.

Lin, M.H., Chen, T.C., Kuo, T.T., Tseng, C.C., and Tseng, C.P. (2000). Real-time PCR for quantitative detection of *Toxoplasma gondii*. J. Clin. Microbiol. *38*, 4121–4125. https://doi.org/10.1128/JCM.38.11.4121-4125.2000.

Liu, L., and Duff, K. (2008). A technique for serial collection of cerebrospinal fluid from the cisterna magna in mouse. J. Vis. Exp. *10*, 960. https://doi.org/10.3791/960.

Lopez-Yglesias, A.H., Burger, E., Camanzo, E., Martin, A.T., Araujo, A.M., Kwok, S.F., and Yarovinsky, F. (2021). T-bet-dependent ILC1- and NK cell-derived IFN-gamma mediates cDC1-dependent host resistance against Toxoplasma gondii. PLoS Pathog. *17*, e1008299. https://doi.org/10.1371/journal.ppat.1008299.

Manglani, M., Gossa, S., and McGavern, D.B. (2018). Leukocyte isolation from brain, spinal cord, and meninges for flow cytometric analysis. Curr. Protoc. Immunol. *121*, e44. https://doi.org/10.1002/cpim.44.

Matta, S.K., Rinkenberger, N., Dunay, I.R., and Sibley, L.D. (2021). *Toxoplasma gondii* infection and its implications within the central nervous system. Nat. Rev. Microbiol. *19*, 467–480. https://doi.org/10.1038/s41579-021-00518-7.

McFarland, A.P., Yalin, A., Wang, S.Y., Cortez, V.S., Landsberger, T., Sudan, R., Peng, V., Miller, H.L., Ricci, B., David, E., et al. (2021). Multi-tissue single-cell analysis deconstructs the complex programs of mouse natural killer and type 1 innate lymphoid cells in tissues and circulation. Immunity *54*, 1320–1337.e4. https://doi.org/10.1016/j.immuni.2021.03.024.

Mohle, L., Israel, N., Paarmann, K., Krohn, M., Pietkiewicz, S., Muller, A., Lavrik, I.N., Buguliskis, J.S., Schott, B.H., Schluter, D., et al. (2016). Chronic *Toxoplasma gondii* infection enhances beta-amyloid phagocytosis and clearance by recruited monocytes. Acta Neuropathol. Commun. *4*, 25. https://doi.org/10.1186/s40478-016-0293-8.

Mrdjen, D., Pavlovic, A., Hartmann, F.J., Schreiner, B., Utz, S.G., Leung, B.P., Lelios, I., Heppner, F.L., Kipnis, J., Merkler, D., et al. (2018). High-dimensional single-cell mapping of central nervous system immune cells reveals distinct myeloid subsets in health, aging, and disease. Immunity *48*, 380–395.e6. https://doi.org/10.1016/j.immuni.2018.01.011.

Nabekura, T., Riggan, L., Hildreth, A.D., O'Sullivan, T.E., and Shibuya, A. (2020). Type 1 innate lymphoid cells protect mice from acute liver injury via interferon-gamma secretion for upregulating Bcl-xL expression in hepatocytes. Immunity *52*, 96–108.e9. https://doi.org/10.1016/j.immuni.2019.11.004.

Narni-Mancinelli, E., Chaix, J., Fenis, A., Kerdiles, Y.M., Yessaad, N., Reynders, A., Gregoire, C., Luche, H., Ugolini, S., Tomasello, E., et al. (2011). Fate mapping analysis of lymphoid cells expressing the NKp46 cell surface receptor. Proc. Natl. Acad. Sci. U S A *108*, 18324–18329. https://doi.org/10.1073/pnas.1112064108.

Oldenhove, G., Bouladoux, N., Wohlfert, E.A., Hall, J.A., Chou, D., Dos Santos, L., O'Brien, S., Blank, R., Lamb, E., Natarajan, S., et al. (2009). Decrease of Foxp3+ Treg cell number and acquisition of effector cell phenotype during lethal infection. Immunity *31*, 772–786. https://doi.org/10.1016/j.immuni.2009.10.001.

Park, E., Patel, S., Wang, Q., Andhey, P., Zaitsev, K., Porter, S., Hershey, M., Bern, M., Plougastel-Douglas, B., Collins, P., et al. (2019). *Toxoplasma gondii* infection drives conversion of NK cells into ILC1-like cells. Elife *8*, e47605. https://doi.org/10.7554/eLife.47605.

Reinhardt, R.L., Liang, H.E., and Locksley, R.M. (2009). Cytokine-secreting follicular T cells shape the antibody repertoire. Nat. Immunol. *10*, 385–393. https://doi.org/10.1038/ni.1715.

Robben, P.M., LaRegina, M., Kuziel, W.A., and Sibley, L.D. (2005). Recruitment of Gr-1+ monocytes is essential for control of acute toxoplasmosis. J. Exp. Med. *201*, 1761–1769. https://doi.org/10.1084/jem.20050054.

Romero-Suarez, S., Del Rio Serrato, A., Bueno, R.J., Brunotte-Strecker, D., Stehle, C., Figueiredo, C.A., Hertwig, L., Dunay, I.R., Romagnani, C., and Infante-Duarte, C. (2019). The central nervous system contains ILC1s that differ from NK cells in the response to inflammation. Front Immunol. *10*, 2337. https://doi.org/10.3389/fimmu.2019.02337.

Samson, S.I., Richard, O., Tavian, M., Ranson, T., Vosshenrich, C.A., Colucci, F., Buer, J., Grosveld, F., Godin, I., and Di Santo, J.P. (2003). GATA-3 promotes maturation, IFN-gamma production, and liver-specific homing of NK cells. Immunity *19*, 701–711. https://doi.org/10.1016/s1074-7613(03)00294-2.

Schindelin, J., Arganda-Carreras, I., Frise, E., Kaynig, V., Longair, M., Pietzsch, T., Preibisch, S., Rueden, C., Saalfeld, S., Schmid, B., et al. (2012). Fiji: an open-source platform for biological-image analysis. Nat. Methods *9*, 676–682. https://doi.org/10.1038/nmeth.2019.

Schulthess, J., Meresse, B., Ramiro-Puig, E., Montcuquet, N., Darche, S., Begue, B., Ruemmele, F., Combadiere, C., Di Santo, J.P., Buzoni-Gatel, D., and Cerf-Bensussan, N. (2012). Interleukin-15-dependent NKp46+ innate lymphoid cells control intestinal inflammation by recruiting inflammatory monocytes. Immunity *37*, 108–121. https://doi.org/10.1016/j.immuni.2012.05.013.

Schwartz, M., and Baruch, K. (2014). The resolution of neuroinflammation in neurodegeneration: leukocyte recruitment via the choroid plexus. EMBO J. *33*, 7–22. https://doi.org/10.1002/embj.201386609.

Sheikh, A., and Abraham, N. (2019). Interleukin-7 receptor alpha in innate lymphoid cells: more than a marker. Front. Immunol. *10*, 2897. https://doi.org/10.3389/fimmu.2019.02897.

Snyder, L.M., and Denkers, E.Y. (2020). From initiators to effectors: roadmap through the intestine during encounter of toxoplasma gondii with the mucosal immune system. Front. Cell Infect. Microbiol. *10*, 614701. https://doi.org/10.3389/fcimb.2020.614701.

Spits, H., Artis, D., Colonna, M., Diefenbach, A., Di Santo, J.P., Eberl, G., Koyasu, S., Locksley, R.M., McKenzie, A.N., Mebius, R.E., et al. (2013). Innate lymphoid cells–a proposal for uniform nomenclature. Nat. Rev. Immunol. *13*, 145–149. https://doi.org/10.1038/nri3365.

Suzuki, Y. (2020). The immune system utilizes two distinct effector mechanisms of T cells depending on two different life cycle stages of a single pathogen, *Toxoplasma gondii*, to control its cerebral infection. Parasitol. Int. *76*, 102030. https://doi.org/10.1016/j.parint.2019.102030.

Suzuki, Y., Orellana, M.A., Schreiber, R.D., and Remington, J.S. (1988). Interferon-gamma: the major mediator of resistance against *Toxoplasma gondii*. Science *240*, 516–518.

Taylor, G.A., Collazo, C.M., Yap, G.S., Nguyen, K., Gregorio, T.A., Taylor, L.S., Eagleson, B., Secrest, L., Southon, E.A., Reid, S.W., et al. (2000). Pathogen-specific loss of host resistance in mice lacking the IFN-gamma-inducible gene IGTP. Proc. Natl. Acad. Sci. U S A *97*, 751–755. https://doi.org/10.1073/pnas.97.2.751.

Van Hove, H., Martens, L., Scheyltjens, I., De Vlaminck, K., Pombo Antunes, A.R., De Prijck, S., Vandamme, N., De Schepper, S., Van Isterdael, G., Scott, C.L., et al. (2019). A single-cell atlas of mouse brain macrophages reveals unique transcriptional identities shaped by ontogeny and tissue environment. Nat. Neurosci. *22*, 1021–1035. https://doi.org/10.1038/s41593-019-0393-4.

Vivier, E., Artis, D., Colonna, M., Diefenbach, A., Di Santo, J.P., Eberl, G., Koyasu, S., Locksley, R.M., McKenzie, A.N.J., Mebius, R.E., et al. (2018). Innate lymphoid cells: 10 Years on. Cell *174*, 1054–1066. https://doi.org/10.1016/j.cell.2018.07.017.

Weizman, O.E., Adams, N.M., Schuster, I.S., Krishna, C., Pritykin, Y., Lau, C., Degli-Esposti, M.A., Leslie, C.S., Sun, J.C., and O'Sullivan, T.E. (2017). ILC1 confer early host protection at initial sites of viral infection. Cell *171*, 795–808.e12. https://doi.org/10.1016/j.cell.2017.09.052.

Xiao, J., Li, Y., Yolken, R.H., and Viscidi, R.P. (2018). PD-1 immune checkpoint blockade promotes brain leukocyte infiltration and diminishes cyst burden in a mouse model of Toxoplasma infection. J. Neuroimmunol. *319*, 55–62. https://doi.org/10.1016/j.jneuroim.2018.03.013.

Yarovinsky, F. (2014). Innate immunity to *Toxoplasma gondii* infection. Nat. Rev. Immunol. *14*, 109–121. https://doi.org/10.1038/nri3598.

Zelco, A., Rocha-Ferreira, E., Nazmi, A., Ardalan, M., Chumak, T., Nilsson, G., Hagberg, H., Mallard, C., and Wang, X. (2020). Type 2 innate lymphoid cells accumulate in the brain after hypoxia-ischemia but do not contribute to the development of preterm brain injury. Front. Cell. Neurosci. *14*, 249. https://doi.org/10.3389/fncel.2020.00249.

Zhu, J., Jankovic, D., Oler, A.J., Wei, G., Sharma, S., Hu, G., Guo, L., Yagi, R., Yamane, H., Punkosdy, G., et al. (2012). The transcription factor T-bet is induced by multiple pathways and prevents an endogenous Th2 cell program during Th1 cell responses. Immunity *37*, 660–673. https://doi.org/10.1016/j.immuni.2012.09.007.

Zhu, Y., Ju, S., Chen, E., Dai, S., Li, C., Morel, P., Liu, L., Zhang, X., and Lu, B. (2010). T-bet and eomesodermin are required for T cell-mediated antitumor immune responses. J. Immunol. *185*, 3174–3183. https://doi.org/10.4049/jimmunol.1000749.

STAR★METHODS

KEY RESOURCES TABLE

REAGENT or RESOURCE	SOURCE	IDENTIFIER
Antibodies		
Asialo GM1 Polyclonal Antibody, Functional Grade	ThermoFisher Scientific	Cat#16-6507-39; RRID:AB_10718540
CD11b (clone M1/70), APC-Cy7	BioLegend	Cat#101226; RRID:AB_830642
CD11b (clone M1/70), APC-eFluor 780	ThermoFisher Scientific	Cat#47-0112-82; RRID:AB_1603193
CD11b (clone M1/70), Brilliant Violet 605	BioLegend	Cat#101257; RRID:AB_2565431
CD11c (clone N418), Brilliant Violet 510	BioLegend	Cat#117353; RRID:AB_2686978
CD16/32 (clone 93), purified	BioLegend	Cat#101302; RRID:AB_312801
CD16/CD32 (clone 93),	ThermoFisher Scientific	Cat#14-0161-86; RRID:AB_467135
CD19 (clone 6D5), Brilliant Violet 510	BioLegend	Cat#115545; RRID:AB_2562136
CD200R (clone OX-110), APC	BioLegend	Cat#123916; RRID:AB_2810379
CD3 (clone 17A2), APC	BioLegend	Cat#100236; RRID:AB_2561456
CD3ε (clone 145-2C11), Brilliant Violet 510	BioLegend	Cat#100353; RRID:AB_2565879
CD4 (clone RM4-5), APC-Cy7	BioLegend	Cat#100526; RRID:AB_312727
CD45 (clone 30-F11), Alexa Fluor 488	BioLegend	Cat#103122; RRID:AB_493531
CD45 (clone 30-F11), Alexa Fluor 700	BioLegend	Cat#103128; RRID:AB_493715
CD45 (clone 30-F11), Brilliant Violet 750	BioLegend	Cat#103157; RRID:AB_2734155
CD45.2 (clone 104), APC-eFluor 780	ThermoFisher Scientific	Cat#47-0454-82; RRID:AB_1272175
CD49a (clone Ha31/8), PE	BD Bioscience	Cat#562115; RRID:AB_11153117
CD49b (clone DX5), PE-Cy7	BioLegend	Cat#108922; RRID:AB_2561460
CD5 (clone 53-7.3), Brilliant Violet 510	BioLegend	Cat#100627; RRID:AB_2563930
CD8a (clone 53-6.7), Alexa Fluor 700	BioLegend	Cat#100729; RRID:AB_493702
CD8a (clone 53-6.7), Brilliant Violet 510	BioLegend	Cat#100751; RRID:AB_2561389
CXCR6 (clone SA051D1)	BioLegend	Cat#151111; RRID:AB_2721558
Eomes (clone Dan11mag), Alexa Fluor 488	ThermoFisher Scientific	Cat#53-4875-82; RRID:AB_10854265
Eomes (clone Dan11mag), PerCP-eFluor 710	ThermoFisher Scientific	Cat#46-4875-82; RRID:AB_10597455
F(ab')2-Goat anti-Mouse IgG (H+L) Secondary Antibody	ThermoFisher Scientific	Cat#A24514; RRID:AB_2535983
GATA 3 (clone TWAJ), Alexa Fluor 488	ThermoFisher Scientific	Cat#53-9966-42; RRID:AB_2574493
GATA 3 (clone TWAJ), PE	ThermoFisher Scientific	Cat#12-9966-42; RRID:AB_1963600
Gr-1 (clone RB6-8C5), Brilliant Violet 510	BioLegend	Cat#108457; RRID:AB_2650931
IFN-γ (clone: XMG1.2), PE-Dazzle594	BioLegend	Cat#505846; RRID:AB_2563980
InVivoPlus anti-mouse NK1.1 (clone PK136)	BioXcell	Cat#BP0036; RRID:AB_1107737
InVivoPlus mouse IgG2a isotype control (clone C1.18.4)	BioXcell	Cat#BP0085; RRID:AB_1107771
Ly6C (clone HK1.4), FITC	BioLegend	Cat#128005; RRID:AB_1186134
Ly6C (clone HK1.4), PE-Cy7	BioLegend	Cat#128017; RRID:AB_1732093
NK1.1 (clone PK136), Brilliant Violet 605	BioLegend	Cat#108753; RRID:AB_2686977
NK1.1 (clone PK136), PE-Cy7	ThermoFisher Scientific	Cat#25-5941-82; RRID:AB_469665
NKp46 (clone 29A1.4), Brilliant Violet 421	BioLegend	Cat#137612; RRID:AB_2563104
NKp46 (clone 29A1.4), PerCP-Cy5.5	BioLegend	Cat#137610; RRID:AB_10641137
Rabbit IgG Isotype Control	ThermoFisher Scientific	Cat#31235; RRID:AB_243593
RORγt (clone B2D), APC	ThermoFisher Scientific	Cat#17-6981-82; RRID:AB_2573254
RORγt (clone B2D), PE	ThermoFisher Scientific	Cat#12-6981-82, RRID:AB_10807092
TNF (clone: MP6-XT22), Brilliant Violet 605	BioLegend	Cat#506329; RRID:AB_11123912
TNF (clone: MP6-XT22), FITC	BioLegend	Cat#11-7321-81; RRID:AB_465417

(*Continued on next page*)

Continued

REAGENT or RESOURCE	SOURCE	IDENTIFIER
Chemicals, peptides, and recombinant proteins		
Collagenase D	Roche	Cat#11088866001
Collagenase from Clostridium histolyticum	Sigma-Aldrich	Cat#C2139
Collagenase type IV	STEMCELL Technologies	Cat#07426
Deoxyribonuclease I	Sigma-Aldrich	Cat#DN25
Dispase® II (neutral protease, grade II)	Roche	Cat#4942078001
peqGOLD total RNA kit	Peqlab	Cat#12-6634-02
peqGOLD TriFast	Peqlab	Cat#30-2010
ProLong™ Gold Antifade Mountant with DAPI	ThermoFisher Scientific	Cat#P36931
RBC Lysis Buffer (10X)	BioLegend	Cat#420301
RNAlater®	Sigma-Aldrich	Cat#R0901
RNA-Solv® Reagent	Omega Bio-Tek	Cat#R6830
Tissue Tek O.C.T. Compound	Sakura Finetek	Cat#4583
TRIzol™ Reagent	ThermoFisher Scientific	Cat#15596026
Critical commercial assays		
Brefeldin A Solution (1,000X)	BioLegend	Cat#420601
Cell Activation Cocktail (without Brefeldin A)	BioLegend	Cat#423302
FastStart Essential DNA Green Master	Roche	Cat#06402712001
Foxp3/Transcription Factor Staining Buffer Set	ThermoFisher Scientific	Cat#00-5523-00
IMDM, GlutaMAX™	ThermoFisher Scientific	Cat#31980030
InVivoPure pH 7.0 Dilution Buffer	BioXcell	Cat#IP0070
Monensin Solution (1,000X)	BioLegend	Cat#420701
peqGOLD total RNA kit	Peqlab	Cat#12-6634-02
TaqMan™ RNA-to-C_T™ *1-Step* Kit	ThermoFisher Scientific	Cat#4392938
Zombie NIR™ Fixable Viability Kit	BioLegend	Cat#423106
Zombie Violet™ Fixable Viability Kit	BioLegend	Cat#423114
Zombie Yellow™ Fixable Viability Kit	BioLegend	Cat#423104
Experimental models: Organisms/strains		
Mouse: B6(Cg)-Ncr1$^{tm1.1(icre)Viv}$/J	(Narni-Mancinelli et al., 2011)	MGI:5308410
Mouse: B6.129S1(Cg)-*Eomes*$^{tm1.1Bflu}$/J	(Zhu et al., 2010)	Strain #017293, MGI:5141850
Mouse: B6.129S4-*Ifng*$^{tm3.1Lky}$/J	(Reinhardt et al., 2009)	Strain #017581, MGI:5317425
Mouse: C57BL/6JRj	Janvier Laboratories	Cat#SC-C57J-F
Mouse: Gata3$^{tm1.1Mbu}$/J	(Amsen et al., 2007; Grote et al., 2006)	Strain #028103, MGI:3719568
Mouse: T-bet-ZsGreen	(Zhu et al., 2012)	MGI:5690118
T. gondii, type II ME 49 strain	(Liesenfeld et al., 2004)	N/A
Oligonucleotides		
Primer Tg.B1 forward: TCCCCTCTGCT GGCGAAAAGT	(Lin et al., 2000)	N/A
Primer Tg.B1 reverse: AGCGTTCGTGG TCAACTATCGATTG	(Lin et al., 2000)	N/A
Primer Mm.ASL forward: TCTTCGTTAGC TGGCAACTCACCT	(Butcher et al., 2011)	N/A
Primer Mm.ASL reverse: ATGACCCAGCA GCTAAGCAGATCA	(Butcher et al., 2011)	N/A
RT-qPCR TaqMan Probes	ThermoFisher Scientific	Table S1
Software and algorithms		
FIJI	(Schindelin et al., 2012)	RRID:SCR_003070
FlowJo	Becton, Dickinson and Company	RRID:SCR_008520
Prism	GraphPad	RRID:SCR_002798

(*Continued on next page*)

Continued

REAGENT or RESOURCE	SOURCE	IDENTIFIER
Other		
Attune NxT Flow Cytometer	ThermoFisher Scientific	RRID:SCR_019590
LightCycler 96 Instrument	Roche	Cat#05815916001
SP6800 spectral cell analyzer	Sony Biotechnology	RRID:SCR_018067

RESOURCE AVAILABILITY

Lead contact

Further information and requests for resources and reagents should be directed to and will be fulfilled by the lead contact, Ildiko Rita Dunay (Ildikodunay@gmail.com).

Materials availability

This study did not generate new unique reagents.

Data and code availability

All data reported in this paper will be shared by the lead contact upon request.

This paper does not report original code.

Any additional information required to reanalyze the data reported in this paper is available from the lead contact upon request.

EXPERIMENTAL MODEL AND SUBJECT DETAILS

Mice

Experiments were conducted with female and male, wild-type C57BL/6JRj (B6/WT) mice (8-16 weeks old), *NKp46*$^{Cre/wt}$*Eomes*$^{flox/flox}$ (8-16 weeks old) (Zhu et al., 2010; Narni-Mancinelli et al., 2011), *NKp46*$^{Cre/wt}$*Gata3*$^{flox/flox}$ (8-16 weeks old) (Amsen et al., 2007; Grote et al., 2006; Narni-Mancinelli et al., 2011), IFN-γ-reporter (interferon-gamma reporter with endogenous polyA transcript, Great; 8-16 weeks old) (Reinhardt et al., 2009), and T-bet-reporter mice (T-bet-ZsGreen) (Zhu et al., 2012) bred under specific pathogen-free (SPF) conditions. Genotyping was performed by PCR analysis of tissue biopsies. Throughout the study, *NKp46*$^{Cre/wt}$*Eomes*$^{wt/flox}$ or *NKp46*$^{wt/wt}$*Gata3*$^{flox/flox}$ littermates served as WT controls. All animal experiments were approved by the local authorities, according to German and European legislation.

METHOD DETAILS

T. gondii cysts of the type II ME49 strain were harvested from the brains of female NMRI mice infected by *intraperitoneal* (*i.p.)* administration of *T. gondii* cysts 6-12 months earlier. Isolated brains were mechanically homogenized in 1 mL sterile PBS, and the number of cysts was determined in $\geq$ 80 μL homogenate using a light microscope. Homogenate was diluted in sterile PBS, and animals were infected by *i.p.* administration of two cysts (Mohle et al., 2016). Uninfected control mice were mock-infected with an equal volume of sterile PBS.

Cell depletion

NK1.1^{+} and asialo GM1^{+} cells were depleted using anti-NK1.1 or anti-asialo GM1 antibodies (Ivanova et al., 2019). Depletion was performed by *i.p.* administration of 200 μg anti-NK1.1 or 50 μg anti-asialo GM1 (diluted in InVivoPure pH 7.0 Dilution Buffer) on day 7, 10, and 13 after infection. Control mice received an equal amount of control IgG antibody (IgG2a isotype control or Rabbit IgG Isotype Control).

Organ collection

Mice were sacrificed, peripheral blood samples were collected, and animals were transcardially perfused with 60 mL sterile ice-cold PBS. Cerebrospinal fluid (CSF) was collected from cisterna magna using a stereo microscope and a glass capillary and kept at 4°C until further analysis. Brain (with pia mater), choroid plexus, meninges (dura meninges and partially arachnoid meninges), spleen, liver, and small intestine were removed and stored in sterile ice-cold PBS or RNAlater for further analysis (Dusedau et al., 2019). Samples stored in RNAlater were kept at 4°C overnight and afterwards transferred to -20°C. For immunofluorescence, transcardial perfusion with 60 mL sterile ice-cold PBS was followed by 20 mL of buffered, 4% paraformaldehyde (PFA).

Cell isolation

Isolation of cells was performed as previously described for brain (Dusedau et al., 2019), choroid plexus (Kunis et al., 2013), meninges (Manglani et al., 2018), and cerebrospinal fluid (Liu and Duff, 2008). In short, brain hemispheres were minced with a scalpel, subsequently homogenized in 2 mL dissection buffer (HBSS, supplemented with 50 mM glucose and 13 mM Hepes (pH 7.3)), using a glass potter and filtered through a 70 μm cell strainer. The cell suspension was centrifuged (400 g, 20 min, 4°C), and the cell pellet was resuspended in 10 mL of 70% (v/v) isotonic Percoll (isotonic Percoll: 90% (v/v) Percoll, 10% (v/v) 10x PBS), overlayered with 10 mL of 30% (v/v) isotonic Percoll and 5 mL of PBS. After removing myelin debris, cells (interface between 70% and 30% isotonic Percoll) were washed with PBS. The supernatant was removed, the cell pellet was resuspended and used for further analysis. For analysis of choroid plexus and brain parenchyma, choroid plexus was removed an processed separately. Brain parenchyma was processed as described above. Isolated choroid plexuses were washed with HBSS, centrifuged (300 g, 2 min, 4°C), and resuspended in 250 μL HBSS containing 400 U/mL collagenase type IV, incubated (600 rpm, 45 min, 37°C), homogenized by pipetting, and passed through 70 μm cell strainer. Cells were washed twice in 1 mL of RPMI containing 5% FCS, centrifuged (400 g, 10 min, 4°C), and pooled (n=2-5 animals per sample) for staining. Isolated meninges were resuspended in 650 μL PBS containing 1 mg/mL DNase I and 1.4 mg/mL collagenase and incubated (300 rpm, 20 min, 37°C). The digestion was stopped with an excess volume of PBS (supplemented with 2 mM EDTA), cells were separated by repeated up/down pipetting, subsequently filtered through a 70 μm cell strainer, and centrifuged (400 g, 7 min, 4°C). Cell pellet was resuspended, cell number was determined, and samples were pooled (n=2-5 animals per sample) for staining. CSF was centrifuged (400 g, 5 min, 4°C), macroscopically assessed for blood contamination, and pooled (n=2-5 animals per sample) for staining where necessary.

Isolation of lamina propria lymphocytes was performed as previously described (Bank et al., 2020; Klose et al., 2014) with minor changes. In short, Peyer's patches were removed, the small intestine was cleaned from remaining fat tissue, opened longitudinally, and subsequently washed using ice-cold PBS containing 100 U/mL penicillin/streptomycin. Epithelial cells were dissociated by incubation (RT, 2×20 min at 100 rpm rotation on a shaking incubator) in dissociation buffer (HBSS w/o Ca^{2+} and Mg^{2+}, 10 mM HEPES, 5 mM EDTA, 1 mM dithiothreitol) and vortexing for 15 s. Tissue was washed with PBS/ Pen/Strep, minced with scissors, and digested in digestion buffer (RPMI with 4% FCS, supplemented with 0.25 mg/mL of DNase I, 0.25 mg/mL Collagenase D, and 0.2 mg/mL Dispase II on a shaking incubator (100 rpm, 2x15 min, 37°C) followed by 15 s vortexing and filtering through 100 μm cell strainers. Finally, leukocytes were filtered through 40 μm cell strainers and further enriched by Percoll gradient centrifugation. 3 mL of 80% (v/v) isotonic Percoll was overlayered with 5 mL of 44% (v/v) isotonic Percoll. Finally, the cell pellet was resuspended in 5 mL of 30% (v/v) isotonic Percoll and added onto the 44% Percoll. Samples were centrifuged (600 g, 20 min, RT, minimal acceleration/deceleration), and cells from the 80%/44% interphase were harvested. Cells were washed with PBS (supplemented with 2 mM EDTA) and centrifuged (600 g, 10 min, 4°C). To isolate immune cells from the liver, organs were homogenized by passage through a 70 μm cell strainer and further enriched by Percoll gradient centrifugation as described above for cell isolation from the brain using 10 mL of 70% (v/v) isotonic Percoll, 10 mL of 35% (v/v) isotonic Percoll and 5 mL of PBS. Immune cells from spleens were isolated by passage through a 40 μm cell strainer. Erythrocytes in the blood and spleen samples were lysed using RBC lysis buffer, subsequently washed with PBS, and centrifuged (400 g, 10 min, 4°C).

Flow cytometric analysis

Cells were resuspended in fluorescence-activated cell sorting (FACS) buffer (PBS, supplemented with 2% (v/v) FCS and 2 mM EDTA) and subsequently stained. In short, cells were incubated with an anti-mouse CD16/32 antibody for 20 min at 4°C. Subsequently, cells were stained using fluorochrome-conjugated antibodies against lineage markers: CD3ε, CD5, CD8a, CD11c, CD19, Gr-1, and a selection of cell surface markers: CD45, CD11b, NK1.1, NKp46, CD49a, CD49b, CXCR6, CD200R, Ly6C, CD84, and CD8a in FACS buffer for 30 min at 4°C, washed twice with FACS-buffer, and centrifuged (400 g, 10 min 4°C). Cells were stained with a fixable viability dye, washed twice with PBS, and fixed overnight using fixation/permeabilization buffer (Foxp3 / Transcription Factor Staining Buffer Set). Cells were washed twice with permeabilization buffer (Foxp3 / Transcription Factor Staining Buffer Set), centrifuged (500 g, 10 min 4°C), and stained using fluorochrome-conjugated antibodies against intracellular markers: GATA-3, RORγt, and Eomes for 40 min at 4°C, washed twice with permeabilization buffer and resuspended in FACS buffer for acquisition. Fluorescence Minus One (FMO) controls were used to assess the level of background fluorescence in the respective detection channel. Expression of cytokines was assessed by *ex vivo* restimulation with Phorbol-12-myristat-13-acetat (PMA) and ionomycin. In short, $5x10^5$ cells were resuspended in 225 μL IMDM, supplemented with 10% FCS and 1% Pen/Strep, and stimulated using 1 μg/mL Ionomycin and 50 ng/mL PMA (Cell Activation Cocktail) for 4 h at 37°C, 5% CO_2. 2 h after the start of the stimulation, a combination of Brefeldin A (5 μg/mL) and monensin (2 μM) was added. Cells were stained as described above, using antibodies against IFN-γ and TNF. Cells were acquired using an SP6800 spectral cell analyzer or Attune NxT Flow Cytometer. Data were analyzed using FlowJo software.

RNA, DNA isolation and RT-qPCR

Samples were removed from RNAlater and homogenized in TRIzol, TriFast, or RNA-Solv using Zirconium oxide beads, BashingBead Lysis Tubes, and BeadBug 6 homogenizer. DNA was isolated from the homogenate according to the manufacturer's instructions. RNA was isolated from the homogenate by isopropanol precipitation or using peqGOLD total RNA kit following the manufacturer's instructions. Analysis of *T. gondii* burden was determined using the FastStart Essential DNA Green Master kit and *T. gondii B1* (*Tg.B1*) as target and mus musculus argininosuccinate lyase (*Mm.Asl*) as reference in a LightCycler 96 instrument. To analyze gene

expression, commercially available gene-specific Taqman probes for interferon gamma (*Ifng*), tumor necrosis factor (*Tnf*), interleukin 15 (*Il15*), transforming growth factor beta 1 (*Tgfb1*), interleukin 7 (*Il7*), interferon regulatory factor 8 (*Irf8*), immunity-related GTPase family M member 1 (*Irgm1*), interferon gamma induced GTPase (*Igtp*), chemokine (C-C motif) ligand 2 (*Ccl2*), chemokine (C-C motif) ligand 3 (*Ccl3*), and the TaqMan™ RNA-to-CT™ 1-Step Kit were used to amplify target genes of interest in a LightCycler 96 instrument. Relative target gene expression to the arithmetic mean of reference gene hypoxanthine guanine phosphoribosyl transferase (*Hprt*) was determined using this formula: $2^{-\Delta CT}$ where ΔCT = (Ct (Target gene) − Ct (*Hprt*)), as previously described (Lee et al., 2018). Finally, $2^{-\Delta CT}$ values were normalized to the arithmetic mean of the control group.

Immunofluorescence

For immunofluorescent stainings, brains were isolated, post-fixed in 4% PFA overnight, immersed in 30% sucrose solution (PBS supplemented with 30% (w/v) sucrose), mounted, and frozen in embedding medium (O.C.T. Compound). Coronal sections (20 μm) were cut within a specific range of the brain (bregma −1.0 mm to bregma −2.5 mm). Sections were thawed, air-dried, and antigen retrieval was performed (10 mM sodium citrate, 0.1% (v/v) Tween 20, pH 6.0) for 30 min at 90°C. Sections were rinsed with PBS, washed three times (PBS, 0.1% (v/v) Tween 20) for 10 min, blocked (PBS, 5% normal goat serum, 0.2% (v/v) Triton X-100) for 1 h, washed, and additionally blocked with unconjugated F(ab')2-Goat anti-Mouse IgG (H+L) antibody (1:500) in PBS for 60 min. After washing, sections were incubated with the primary antibody anti-CD3-APC (1:50) for 2 h at RT in staining buffer (PBS, 1% normal goat serum, 0.1% (v/v) Triton X-100). Sections were washed three times, covered with Prolong Gold, visualized using a Leica TCS SP8 confocal microscope, and processed using FIJI. Contrast, brightness and color balance were adjusted and images were rotated and cropped where necessary to ensure comparability.

QUANTIFICATION AND STATISTICAL ANALYSIS

The specific tests used to analyze the experiments and sample sizes are indicated in the figure legends. Data were tested for normality using D'Agostino-Pearson ($n \geq 8$) or Shapiro-Wilk normality test ($n < 8$) and equality of variances using F test in advance for selection of the statistical test. Sample sizes for animal experiments were chosen with adequate statistical power based on the literature and previous experience. The investigators were blinded to the identity of the groups during experiments and analysis where possible. Statistical calculations were performed using GraphPad Prism and considered significant if $p \leq 0.05$. Data are presented as the arithmetic mean with the corresponding standard error of the mean (SEM). To ensure visual comparability of markers with considerably differing absolute MFIs in a single heat map (Figure 1C), the MFIs of each marker were normalized (highest value 1, lowest value 0).